Int. J. Electrochem. Sci., 17 **(2022)** Article Number: 22031, doi: 10.20964/2022.03.20

International Journal of
ELECTROCHEMICAL
SCIENCE
www.electrochemsci.org

SnO_2@C composite as Anode Material of Lithium-ion Batteries with Enhanced Cycling Stability

Li-lai Liu[1,2,3,], Ming-yang Li[1], Yi-han Sun[1], Min-xuan Ma[1], Xue-ying Yang[1], Hui Wang[1]*

[1] College of Environmental and Chemical Engineering, Heilongjiang University of Science and Technology, Harbin 150022, China
[2] School of Chemical Engineering and Technology, Harbin Institute of Technology, Harbin, 150001, China
[3] Baotailong new materials co. LTD., Jixi 158100, China
[*]E-mail: lllusth@163.com

Received: 16 September 2021 / *Accepted:* 1 November 2021 / *Published:* 2 February 2022

The SnO_2@C composite was prepared by a two-step microwave-hydrothermal method using a microwave reaction system. The surface of the carbon spheres is composited of the SnO_2 nanoparticles with a diameter of about 3 nm. The SnO_2@C composite exhibits excellent electrochemical performances in lithium-ion batteries. The first discharge/charge capacities at a current density of 700 and 1000 mAg^{-1} is 1393/766 and 1309/685 $mAh \cdot g^{-1}$ with coulomb efficiencies of 54.99% and 52.33%, respectively. Even after 100 cycles, the discharge specific capacities at a current density of 1000 mAg^{-1} remains 480 $mAh \cdot g^{-1}$ with coulomb efficiencies of 99.40%.

Keywords: SnO_2, microwave-hydrothermal, lithium-ion batteries, carbon spheres, electrochemical performances

1. INTRODUCTION

With the rapid development of portable electronics (such as laptops, mobiles, play-stations, etc.) involving lithium-ion batteries as energy storage devices, the demand for lithium-ion batteries (LIBs) in the whole industry is increasing[1-3]. LIBs have potential for a wide range of applications, due to energy density, the advantages of large capacity, high working voltage, long cycle life and so on [4-7]. However, Graphite remains its lower theoretical capacity (only 372 mAh g^{-1}) as an anode material and was hard to meet the demand of the next generation LIBs [8-10]. In consequence, it is necessary to explore new anode materials instead of graphite in order to promote the electrochemical performances and meet the increasing demand for anode.

Tin (Sn) is non-toxic, inexpensive and naturally highly abundant element and is amongst the most important metallic material [11]. In the past several years, Sn-based materials (Sn, SnO_2, etc.) attract considerable attention as a promising anode material because of their intrinsic feasibility, high electrical conductivity, low voltage plateau and appreciable theoretical capacity [12]. SnO_2 has a specific capacity of about 780 mAh g^{-1}, which is more than twice as much as commercialized graphite [13,14].

However, the large volume change (≥300%) produced during the charge/discharge process of lithium, resulting in poor capacity retention and rate capability [15-17]. Its poor ionic and electronic conductivities leading to slow charge/discharge rates[18]. These disadvantages seriously hinder the application of SnO_2 in LIBs.

To alleviate above issues, the excellent conductivity of carbon can effectively improve the conductivity of the electrode material and the transport speed of lithium-ion on the surface of the nanomaterial, and thereby correspondingly promote the cycle performance of the anode material [16,18]. Many research groups adopt carbonaceous materials as a buffer matrix to accommodate the large volume changes of SnO_2, along with a conductivity enhancer [19,20]. It is demonstrated that the carbon-based hosts can buffer the volume expansion of SnO_2 nanoparticles and play crucial roles.

In our work, the SnO_2@C composites are successfully synthesized by a two-step microwave-hydrothermal method and used as anode materials for the lithium-ion batteries. SnO_2 nanoparticles can provide larger specific surface area and increase the Li-ion transport channel. In addition, this experimental material is nano carbon spheres, which is different from our previous work [21]. The carbon spheres not only stabilize SnO_2 nanoparticles, but also buffer the volume expansion of SnO_2 nanoparticles. The obtained SnO_2@C shows excellent the electrochemical performance. Therefore, the SnO_2@C composite is a promising material for energy storage.

2. EXPERIMENTAL

2.1 Preparation of carbon spheres

The carbon spheres was produced from the glucose powder by a microwave hydrothermal method. Firstly, appropiate amount of glucose was dissolved in appropiate amount of deionized water under magnetic stirring for 10min. The resulting solution was transferred into a sealed Teflon-lined stainless steel autoclave of the microwave reaction system. The system temperature, pressure and reaction time were 180 ºC, 2.5 MPa and 120 min. After that, the product was collected and washed by centrifugation with deionized water. Then the sample dried at 100 ºC in vacuum drying oven and then grounded into a powder to obtain carbon spheres.

2.2 Preparation of SnO_2@C

Firstly, 200 mL 0.04 mol·L^{-1} $SnCl_4$ solution was prepared, 0.1g of the carbon spheres was dissolved in 20 mL of deionized water. Then 8ml, 10ml, 12ml, 14ml $SnCl_4$ solution was added slowly, respectively. The obtained product sonicated for about 30 min to assure the homogeneous dispersion of

the obtained product. The reaction was transferred into a sealed Teflon-lined stainless steel autoclave and conducted for hydrothermal treatment at 180 ºC for 8 h. In order to improve the carbonization degree of SnO_2@C composites, the prepared samples were heat-treated for 120 min at 500 ºC under nitrogen gas.

2.3 Sample characterization

The materials were characterized by scanning electron microscope (SEM, Quanta 200F), transmission electron microscopy (TEM, FEI TECNAI G2 F20), X-ray diffraction (XRD, Bruker D8 Advance with Cu Kα radiation) operated at 40 kV and 40 mA, Raman (Renishaw RM-1000) were recorded in a plus laser Raman spectrometer with an excitation laser beam wavelength of 514.5 nm, FT-IR analysis was carried out using pressed KBr disks in the range 4000-400 cm^{-1} with a PerkinElmer spectrometer.

2.4 Electrochemical measurements

The electrochemical measurements were carried out using CR2025 coin-type cells. The working electrode was prepared by the method reported in our previous work, which was coating slurry consisting of active material, PVDF (polyvinylidene fluoride) and acetylene black with a weight ratio of 80:10:10 in NMP (N-methyl-pyrrolidone) solvent [21].

3. RESULTS AND DISCUSSION

3.1 Microstructural characterization

Figure 1 is the SEM images of SnO_2@C of the amount of different $SnCl_4$. It can be seen from the figure when the amount of $SnCl_4$ solution is small, the surface of carbon spheres is completely coated by SnO_2 and the coating layer of SnO_2@C is uniform. It can produce spherical solid products with a particle size of about 100 nm. With the increase of $SnCl_4$ solution, the size of SnO_2@C material becomes uneven, the coating layer is not uniform, and the surface of the sphere is rougher. In particular, when 8 mL $SnCl_4$ solution was added, Sn^{4+} could precisely obtain the oxygen in the oxygen-containing functional groups on the surface of the polysaccharide nano carbon spheres and directly nucleated into nano SnO_2 on the surface of the nano carbon spheres. The prepared SnO_2@C composite has the best morphology, the most uniform size and coating layer.

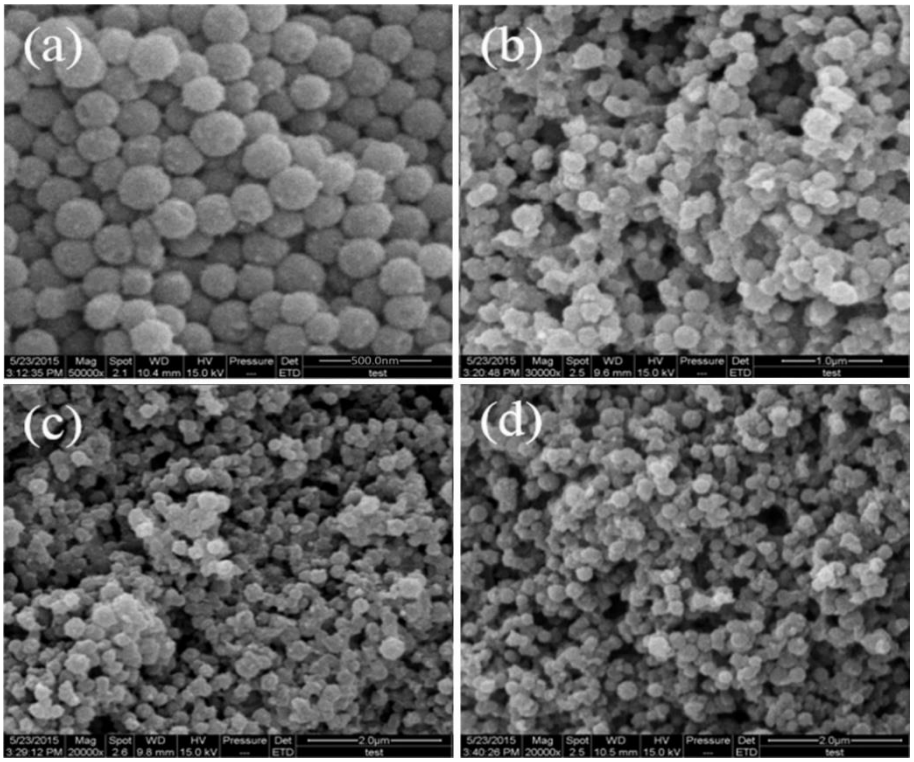

Figure 1. SEM images of SnO_2@ C of the amount of different $SnCl_4$ by hydrothermal treatment at 180 ºC for 8 h (a) 8 mL, (b) 10 mL, (c) 12 mL and (d) 14 mL

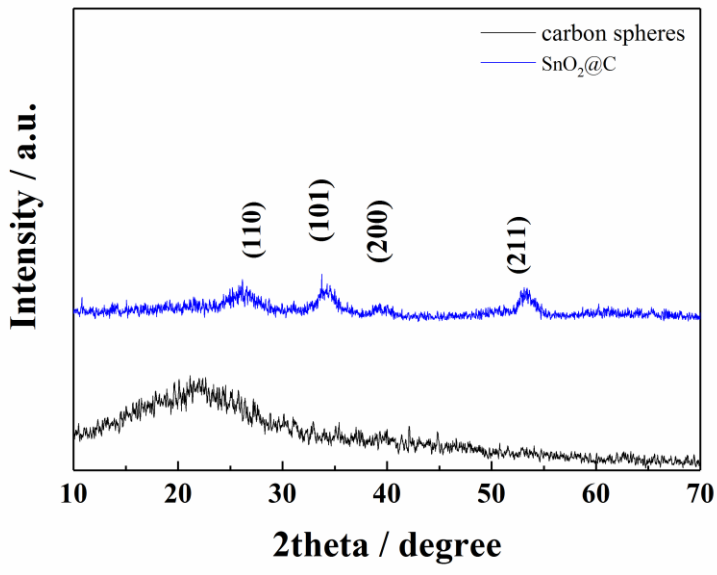

Figure 2. XRD patterns of carbon spheres and SnO_2@C

The X-ray diffraction (XRD) patterns of SnO_2@C are illustrated in figure 2 by two step hydrothermal method. All the diffraction peaks in figure 2 are ascribed to the standard tetragonal SnO_2

phase (JCPDS card No. 00-041-1445) [22], According to JCPDS card (No. 00-041-1445), confirmed the structure of the as-prepared composite and indicated the crystalline SnO_2 nanoparticles can be formed by the microwave-hydrothermal reaction. The diffraction peak of carbon does not appear in this XRD patterns. Because the diffraction peak of carbon spheres are covered by the diffraction peak of SnO_2 nanoparticles, or the diffraction peak of carbon spheres coincides with the diffraction peak of (110) crystal plane of SnO_2.

The Fourier transform infrared (FT-IR) spectra of carbon spheres and SnO_2@C is presented in figure 3. The spectra changed greatly when Carbon spheres were combined with tin source under hydrothermal conditions.

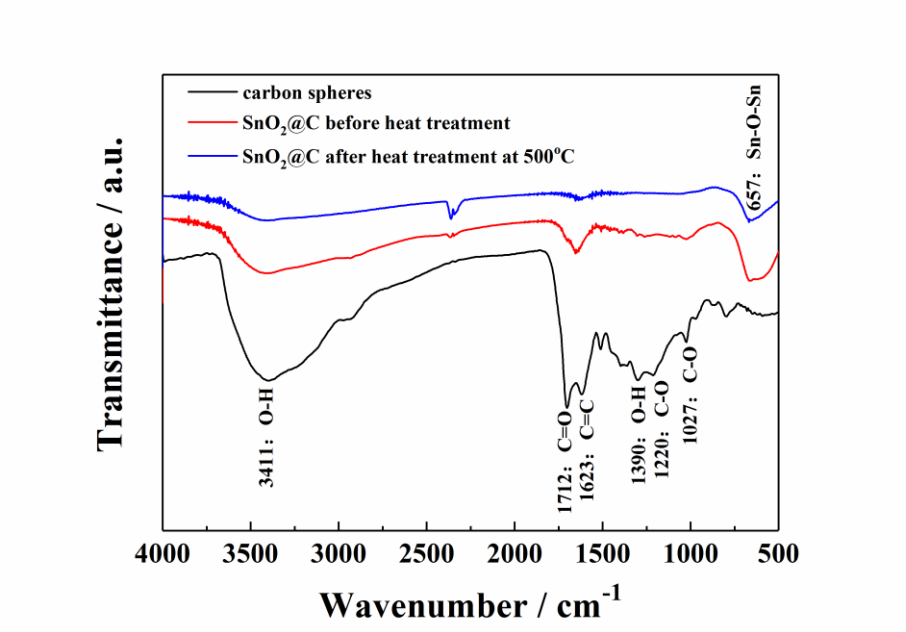

Figure 3. FTIR spectra of carbon spheres and SnO_2@C before heat treatment and after heat treatment at 500 °C

The O-H and C-O absorption peaks at approximately 1390 cm^{-1} and 1220 cm^{-1} almost completely disappeared, the C=O and C-OH peaks at approximately 1721 cm^{-1} and 1027 cm^{-1} decreased significantly, the main peak near 657 cm^{-1} corresponds to the anti-vibration absorption peak of Sn-O-Sn bond [23]. It is indicated that tin ion obtains oxygen in oxygen-containing functional group of polysaccharide nano carbon spheres and generates SnO_2 particles in the hydrothermal reaction. SnO_2@C after heat treatment, the vibration absorption peak of C=O bond near 1712 cm^{-1} and the stretching vibration peak of C-O bond at 1220 cm^{-1} completely disappeared, indicating that SnO_2@C was further carbonized after heat treatment.

The Raman spectra of SnO_2@C before and after heat treatment are shown in figure 4. There are two obvious peaks at approximately 1350 cm^{-1} and 1590 cm^{-1}, which correspond to the D and G peaks of carbon materials, respectively [24]. The ID/IG ratio of SnO_2@C is decreased after heat treatment. It is indicated that the carbon spheres lose oxygen in the oxygen-containing functional groups on the

surface at high temperatures and are further reduced and carbonized, and the disordered Sp^3 carbon atoms are transformed into Sp^2 carbon atoms.

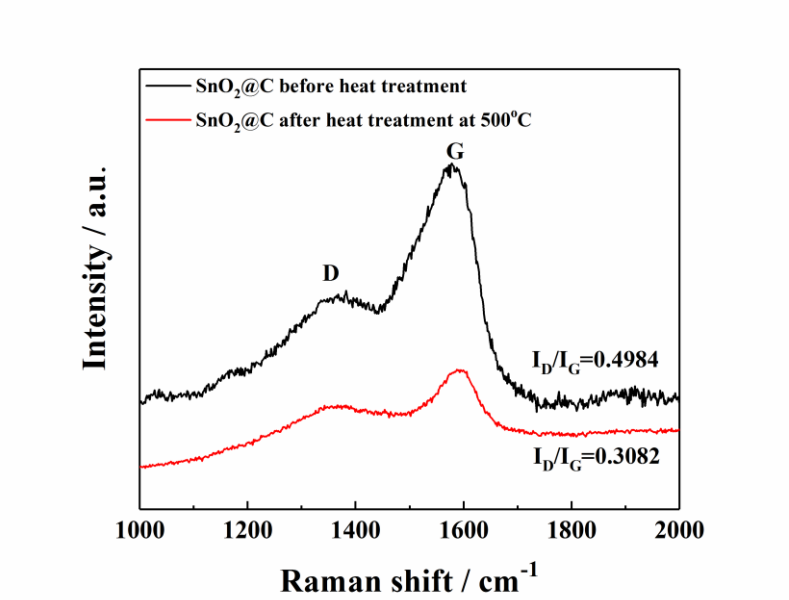

Figure 4. Raman spectra of SnO_2@C before and after heat treatment at 500 °C

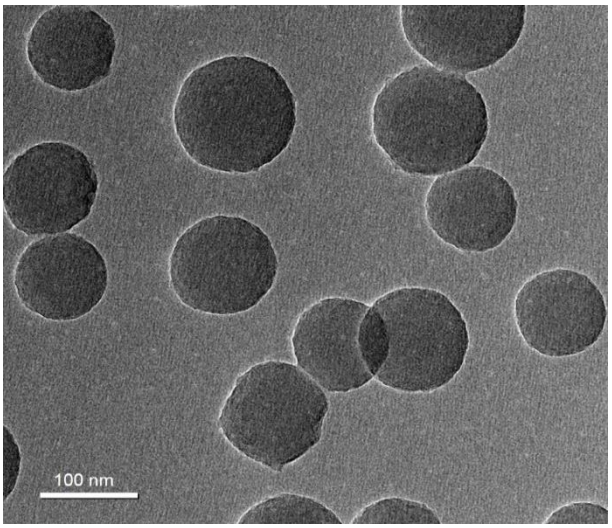

Figure 5. TEM image of carbon spheres

The morphologies of the carbon spheres and the SnO_2@C composite are observed by transmission electron microscopy (TEM) and high resolution transmission electron microscopy (HRTEM). As can be seen from the figure 5, the carbon spheres are solid structure with an average particle size of 80 nm, the surface of the carbon spheres is not completely smooth. From figure 6, the average particle diameter of materials using the microwave-hydrothermal method is 100~120 nm

spheres. Compared with the TEM image of carbon spheres in Fig. 5, the surface of the SnO_2@C became rougher and the diameter of the SnO_2@C became larger. the surface of the spheres is composited of small SnO_2 nanoparticles with a diameter of about 3 nm, and the lattice is clearly visible.

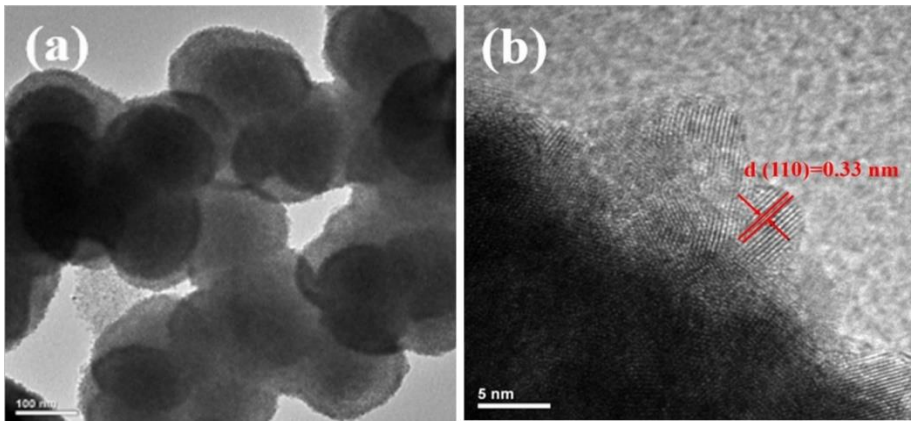

Figure 6. Morphology characterization of SnO_2@C (a) TEM and (b) HRTEM

The composition of SnO_2@C material obtained from the energy dispersive spectroscopy (EDS) is presented in figure 7. Figure 7 shows the general EDS spectrum of SnO_2@C, which reveals the presence of carbon, oxygen and tin. The element content of SnO_2@C is shown in Table 1. According to the table, the mass fractions of C, O and Sn are 38.76%, 13.09% and 48.15% respectively, and the calculated molar ratio of Sn and O is about 1:2, which is consistent with the characterization results of XRD. If only the content of C and O is considered, the mass fraction of C and O is 74.75% and 25.25%, respectively, and the O content in the composite increased due to the addition of SnO_2.

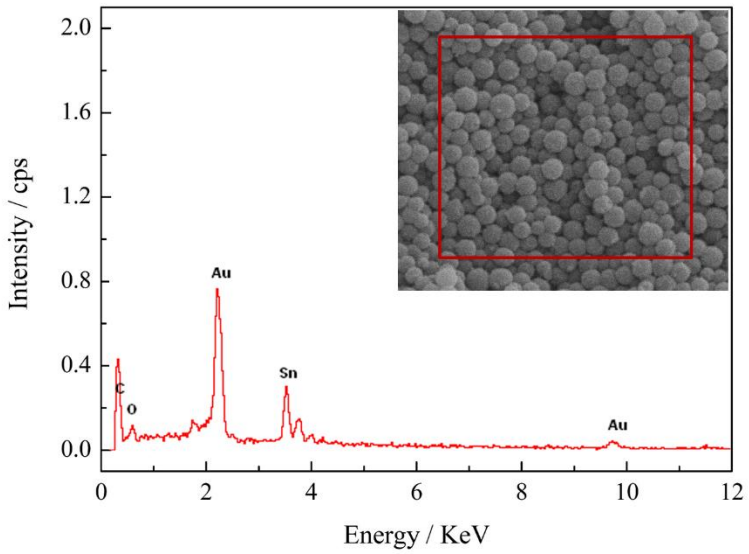

Figure 7. EDS image of SnO_2@C

Table 1. Element content of SnO_2@C

The element	The mass fraction （%）	atomic ratio （%）
C	38.76	72.52
O	13.09	18.37
Sn	48.15	9.11
Matrix	Correction	ZAF

3.2 Electrochemical properties

The LIBs of SnO_2@C composite was studied as an anode material in order to examine the lithium storage performances and mechanism of electrode material. Figure 8 depicts representative discharge and charge curves of SnO_2@C composite at current densities of 700 and 1000 mA g^{-1}, with an operating voltage of 3.0~0.01 V. At a current density of 1000 mA g^{-1}, the initial discharge and charge capacities are 1309 and 685 mAh g^{-1}, respectively, and the first cycle coulomb efficiency is 52.33%. At a current density of 700 mA g^{-1}, the initial discharge and charge capacities are 1393 and 766 mAh g^{-1}, respectively, and the first cycle coulomb efficiency is 54.99%. With decreasing current density, the initial discharge and charge capacities increase, as does the Coulomb efficiency. The research results indicate that low current discharge can significantly reduce the formation of solid electrolyte interface (SEI) and the proportion of irreversible capacity loss caused by SnO_2 reduction during the first charge and discharge process.

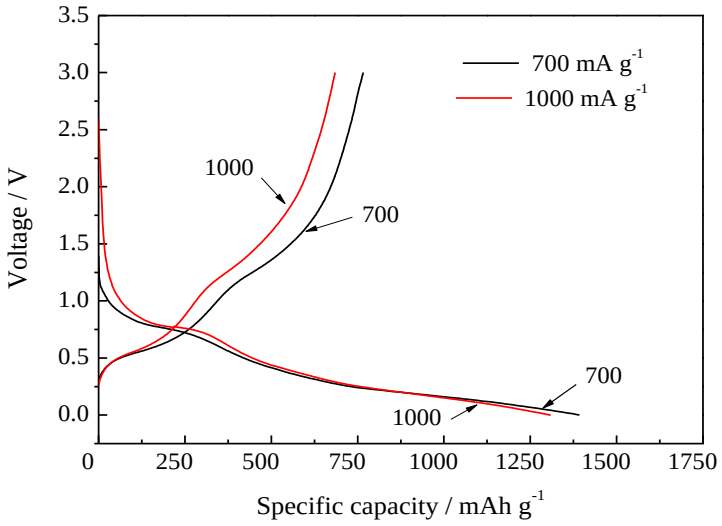

Figure 8. First charge-discharge profiles of SnO_2@C at the current densities of 700 and 1000 mA·g^{-1}

Figure 9 shows Charge-discharge profiles of SnO_2@C cycled for the 1st, 2nd, 10th, 20th, 50th

and 100th cycle at the current densities of 1000 mA·g^{-1}. As presented in Fig. 9. A plateau in the initial discharge at around 0.85 V was observed, relating to the formation of the solid electrolyte interphase (SEI) layer and the decomposition of SnO_2 to become Sn [25,26]. At the beginning of the second charge-discharge cycle, the discharge voltage platform gradually decreases. As the number of cycles increases, the voltage platform becomes less and less obvious and the capacity loss becomes less and less, indicating stable SEI and lithium-ion transport channels are generated.

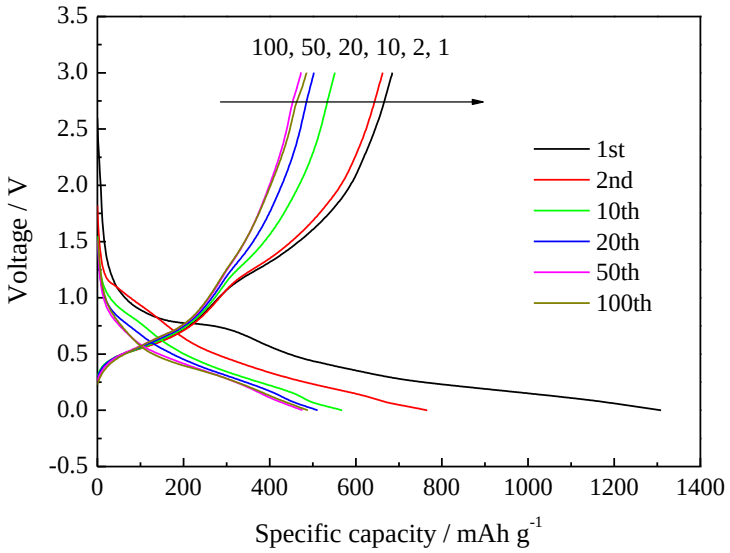

Figure 9. Charge-discharge profiles of SnO_2@C cycled for the 1st, 2nd, 10th, 20th, 50th and 100th cycle at the current densities of 1000 mA·g^{-1}

Figure 10 shows cycle performance and coulombic efficiengcy of SnO_2@C at current densities of 1000 mA g^{-1}. The irreversible capacity loss occurs during the first discharge due to the formation of the SEI on the surface of SnO_2@C electrode material, and the first coulomb efficiency is 52.33%. In the second cycle, the discharge and charge capacities are 685 mAh·g^{-1} and 689 mAh·g^{-1}, respectively, and the coulomb efficiency is obviously improved. The cycling performance of constant charge-discharge tends to be stable in the 20th cycle, and the discharge specific capacities is 496 mAh·g^{-1}. After 100 cycles, the discharge specific capacities at a current density of 1000 mAg^{-1} remains 480 mAh·g^{-1} with coulomb efficiencies of 99.40%. The reversible capacitance and current density of other anode materials in recent studies are compared with the data obtained in our study. As we can see from the Table 2, the reversible capacity obtained in this study is higher than most of the reversible capacities reported using other anode materials. And the SnO_2@C composite fabricated by a facile and two-step hydrothermal method is simpler than other anode materials preparation methods and it does not require high temperature treatment.

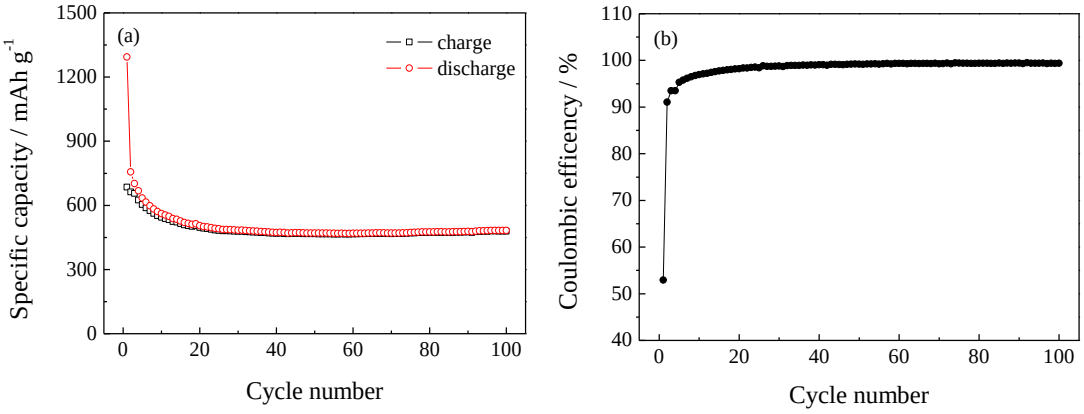

Figure 10. Cycle performance and coulombic efficiengcy of SnO_2@C (a) cycle performance at current densities of 1000 mA g^{-1} and (b) coulombic efficiency

Table 2. Comparison of the electrochemical lithium-storage performance of the SnO_2@C composite presented in this work with previously reported other anode materials.

Materials	Method	Reversible capacity (mA h g^{-1})	Current density	Reference
SnO_2@C	microwave hydrothermal	480 mA h g^{-1}/100th	1000 mA g^{-}	This study
Bi@C nanowires	hydrothermal method	215 mA h g^{-1}/100th	500 mA g^{-1}	[27]
$NiCo_2O_4$/carbon	electrospun	639 mA h g^{-1}/100th	200 mA g^{-1}	[28]
Sn/C composite	calcination method	373.5 mA h g^{-}	100 mA g^{-1}	[29]
$KMnO_4$ and	100 ^{o}C -dried	133 mA h g^{-1}/10th	700 mA g^{-1}	[30]
TiO_2 nanofibers	electrospinning	132.4 mA h g^{-}	500 mA g^{-1}	[31]
Fe/Fe_3C@GC	co-pyrolysis	302 mA h g^{-1}/200th	200 mA g^{-1}	[32]

4. CONCLUSIONS

In summary, the SnO_2@C composite is fabricated by glucose and $SnCl_4 \cdot 5H_2O$ by a simple two-step hydrothermal method. The first discharge/charge capacities at a current density of 700 and 1000 mAg^{-1} is 1393/766 and 1309/685 $mAh \cdot g^{-1}$ with coulomb efficiencies of 54.99% and 52.33%, respectively. Even after 100 cycles, the discharge specific capacities at a current density of 1000 mAg^{-1} remains 480 $mAh \cdot g^{-1}$ with coulomb efficiencies of 99.40%. As an anode materials for lithium-ion batteries, the as-prepared SnO_2@C composite exhibits excellent electrochemical performances. This is related to the size of SnO_2 particles in composite was less than 3.3 nm, which can provide larger specific surface area and increase the lithium-ion transport channel, and the carbon nanospheres with better dispersion and homogeneity structure not only stabilize SnO_2 nanoparticles, but also buffer the volume expansion of SnO_2 nanoparticles. We hope this work can pave the way to obtain electrode materials with high specific capacity, excellent rate capability and stable long-term cycling performance for energy storage.

ACKNOWLEDGEMENT
The work is supported by National Natural Science Foundation of China (no. 51604102), Natural Science Foundation of Heilongjiang Province (no. LH2021B026), and First Class Postdoctoral Fund of Heilongjiang Province (no. LBH-Z16202).

References

1. 1. L. F. Zhou, D. R. Yang, T. Du, H. Gong and W. B. Luo, *Front. Chem.*, 8 (2020) 3412.
2. 2. Y .S. Meng, J. Xin, F. L. Zhu and Y. Zhang, *Int. J. Electrochem. Sci*., 11 (2016) 9881.
3. 3. H. D. Liu, L. Zhang and H. B. Ruan, *Int. J. Electrochem. Sci.*, 13 (2018) 4775.
4. J. W. Choi and D. Aurbach, Nat. Rev. Mater., 1 (2016) 16013.
5. L. W. Ji, Z. Lin, M. Alcoutlabi and X. W. Zhang, *Energ. Environ. Sci.,* 4 (2011) 2682.
6. C. Heubner, T. Liebmann, M. Schneider and A. Michaelis, *Electrochimi. Acta.,* 269 (2018) 745.
7. L. Liu, L. Yang, P. Wang, C. Y. Wang, J. Cheng, G. Zhang, J. J. Gu and F. F. Cao, *Int. J. Electrochem. Sci.*, 12 (2017) 9844.
8. J. J. Luo, J. B. Zhou, D. Lin, Y. Ren and K. B. Tang, *J. Power Sources*., 370 (2017) 14.
9. L. Wen, X. Qin, W. Meng, N. Cao and Z. H. Song, *Mat. Sci. Eng*. B., 213 (2016) 63.
10. H. Jiao, G. B. Lin, H. C. Ping, W. B. Ping, Y. Dan and W. X. Wei, *Int. J. Electrochem. Sci*., 14 (2019) 3455.
11. K. V. Kravchyk, L. Protesescu. M. I. Bodnarchuk, F. Krumeich, M. Yarema, M. Walter, C. Guntlin and M. V. Kovalenko. *J. Am. Chem. Soc*., 135 (2013) 4199.
12. D. D. Han, S. C. Xu, J. J. Li, G. X. Song and Z. D. Guo, *Mater Lett*., 199 (2017) 93.
13. X. W. Lou, C. M. Li, L. A. Archer, *Adv. Mater*., 21 (2009) 2536.
14. L. Xia, S. Q. Wang, G. X. Liu, L. X. Ding, D. D. Li, H. H. Wang and S. Z. Qiao, *Small.*, 12 (2016) 853.
15. C. C. Chang, L. C. Chen, T. Y. Hung, Y. F. Su, H. K. Su, J. H. Lin, C. W. Hu, L. Saravanan and T. Y. Chen, *Int. J. Electrochem. Sci*., 3 (2018) 11762.
16. S. G. Wang, D. Y. Liu, J. J. Yang, G. M. Wang and Q. R. Deng, *Ionics*,. 26 (2020) 5333.
17. X. L. Sun, *Ionics*, 26 (2020) 3841.
18. X. F. Du, T. J. Yang, J. Lin, T. Y. Feng, J. B. Zhu, L. Lu, Y. L. Xu and J. P. Wang, *ACS. Appl. Mater. Inter*., 8 (2016) 15598.
19. S. Oro, K. Urita and I. Moriguchi, *J. Phys. Chem*. C., 20 (2016) 25717.
20. Y. Y. Cheng, J. F. Huang, L. Y. Cao, H. Xie, F. L. Yu, S. H. Xi, B. Y. Shi and J. Y. Li, *ChemElectroChem*., 7 (2020) 1016.
21. L. L. Liu, M. Z. AN, P. X. Yang and J. Q. Zhang, *Sci. Rep.,* 5 (2015) 9055.
22. S. Sathishkumar, M. Parthibavarman, V. Sharmila, M. Karthik, *J. Mater. Sci.: Mater. Electron*., 28 (2017) 8192.
23. S. Suthakaran, S. Dhanapandian, N. Krishnakumar and N. Ponpandian, *J. Phys. Chem. Solids*., 141 (2020) 109407.
24. I. A. Stenina, R. R. Shaydullin, A. V. Desyatov, T. L. Kulova, A. B. Yaroslavtsev, *Electrochim. Acta.*, 364 (2020) 137330.
25. H. Qiao, Z. Zheng, L. Z. Zhang and L. F. Xiao, *J. Mater. Sci*., 43 (2008) 2778.
26. A. C. Ferrari, *Solid. State. Commun*., 143 (2007) 47.
27. Z. Liu, S. M. Jin, K. X. Cui, J. Zhao, S. Y. Xie, J. Z. Li and C. X. Hua, *J. Alloy Compd*., 842 (2020) 155796.
28. M. L. Hsiao and C. T. Lo, *Int. J. Energ. Res*., 44 (2020) 8606.
29. S. Q. Nie, R. Li, Y. Xin, Y. Tan, C. Miao, Y. H. Xiang and W. Xiao, *Solid State Ionics*., 368 (2021) 115703.

30. K. Q. Ding, H. C. Wang, B. J. Wei, Y. Z. Sun, X. M. Shi, C. X. Li, H. Wang, H. M. Dou and J. Q. Pan, *Mater. Chem. Phys*., 213 (2018) 422.
31. J. Li, H. D. Liu, Z. L. Hu, Y. Chen, H. B. Ruan, L. Zhang and R. Hu, *J. Mater. Sci.: Mater. Electron*., 27 (2016) 8682.
32. Y. Liu, X. Y. Li, A. K. Haridas, Y. Z. Sun, J. W. Heo, J. H. Ahn and Y. Lee*, Energies*., 13 (2020) 827.